Immunity
Article

The Histone Methyltransferase Wbp7 Controls Macrophage Function through GPI Glycolipid Anchor Synthesis

Liv Austenaa,[1] Iros Barozzi,[1] Agnieszka Chronowska,[1] Alberto Termanini,[1] Renato Ostuni,[1] Elena Prosperini,[1] A. Francis Stewart,[2] Giuseppe Testa,[1] and Gioacchino Natoli[1,*]
[1]Department of Experimental Oncology, European Institute of Oncology (IEO), Via Adamello 16, 20139 Milan, Italy
[2]Genomics, BioInnovationsZentrum, Technische Universitaet Dresden (TUD), Tatzberg 47, 01307 Dresden, Gerrmany
*Correspondence: gioacchino.natoli@ifom-ieo-campus.it
DOI 10.1016/j.immuni.2012.02.016

SUMMARY

Histone methyltransferases catalyze site-specific deposition of methyl groups, enabling recruitment of transcriptional regulators. In mammals, trimethylation of lysine 4 in histone H3, a modification localized at the transcription start sites of active genes, is catalyzed by six enzymes (SET1a and SET1b, MLL1–MLL4) whose specific functions are largely unknown. By using a genomic approach, we found that in macrophages, MLL4 (also known as Wbp7) was required for the expression of Pigp, an essential component of the GPI-GlcNAc transferase, the enzyme catalyzing the first step of glycosylphosphatidylinositol (GPI) anchor synthesis. Impaired Pigp expression in *Wbp7*$^{-/-}$ macrophages abolished GPI anchor-dependent loading of proteins on the cell membrane. Consistently, loss of GPI-anchored CD14, the coreceptor for lipopolysaccharide (LPS) and other bacterial molecules, markedly attenuated LPS-triggered intracellular signals and gene expression changes. These data link a histone-modifying enzyme to a biosynthetic pathway and indicate a specialized biological role for Wbp7 in macrophage function and antimicrobial response.

INTRODUCTION

The inherent structure of chromatin imposes the need for dedicated mechanisms to control accessibility and usage of the underlying genetic material (Kornberg and Lorch, 1999). At the same time it provides regulatory opportunities that are exploited by eukaryotes to control both differential usage of the genomic information during differentiation and the deployment of specific gene expression programs in response to changing environments. At the heart of this control system are the N-terminal tails of core histones, which undergo a wide array of posttranslational modifications catalyzed by enzymes involved in multiple steps of transcriptional control (Jenuwein and Allis, 2001; Kouzarides, 2007).

Histone tail methylation is dynamically controlled by site-specific methylases and demethylases whose effect on transcription is dependent on which lysine (or arginine) is modified and on the degree of methylation (mono-, di-, or trimethylation) eventually achieved (Cloos et al., 2008; Klose and Zhang, 2007). For instance, trimethylation of K9 and K27 in histone H3 (H3K9me3 and H3K27me3) control transcriptional repression and silencing (Boyer et al., 2006; Bracken et al., 2006; Lee et al., 2006b; Peters et al., 2001), and the interaction between H3K9me3 and HP1 proteins has become the paradigm for the recognition of a histone modification by a specific "reader" in charge of translating the modification into a functional outcome (in this case repression and heterochromatin formation) (Lachner et al., 2001).

In higher eukaryotes, an additional element of complexity is represented by the appearance of multiple paralogs and/or evolutionarily distinct enzymes effecting the same modification. In some cases these paralogs act redundantly, as exemplified by the two heterochromatic H3K9 trimethylases Suv39h1 and Suv39h2 (Peters et al., 2001). However, clear functional differences can usually be seen among evolutionary unrelated enzymes acting on the same site: for instance G9a (also known as Ehmt2) and its dimerization partner (and paralog) Glp (also known as Ehmt1) selectively catalyze H3K9 methylation in euchromatin (Tachibana et al., 2002, 2005), thus demonstrating a different biological function from the heterochromatin-specific Suv39h1 and Suv39h2 (Peters et al., 2003).

H3K4me3 is associated with the transcription start sites (TSS) of active or poised genes (Bernstein et al., 2005; Santos-Rosa et al., 2002) and is detected by several recognition domains present in transcriptional regulators, including the PHD finger, the chromodomain, and the tudor domain (Huang et al., 2006; Kim et al., 2006; Peña et al., 2006; Ruthenburg et al., 2007).

In spite of its correlation with gene activity, the functional role of H3K4me3 is unclear. In vitro data indicate that this modification has no direct effect on transcription (Pavri et al., 2006), and deletion of the only H3K4 methyltransferase in the yeast genome, Set1, has marginal consequences on the transcriptome (Miller et al., 2001). A possible role in tuning splicing rates is suggested by the association of an H3K4me3 binding protein, Chd1, with spliceosome components (Sims et al., 2007). Rather than promoting gene activation, in higher eukaryotes H3K4me3 may prevent inappropriate silencing: in *Drosophila*, deletion of trithorax group H3K4 methyltransferases causes loss of Hox genes expression, which can be rescued by simultaneous deletion of Polycomb group proteins (which control H3K27me3-dependent repression) (Klymenko and Müller, 2004).

In mammals, H3K4me3 deposition is controlled by the Set1-MLL family of enzymes, which includes six members: Set1a and Set1b and MLL1–MLL4. Set-MLL proteins are found in three multimolecular complexes, each one containing either of two highly related paralogs as the catalytically active subunit: the Set1a-Set1b complex, the MLL1-MLL4 complex, and the MLL2-MLL3 complex (Supplemental Discussion available online; Cho et al., 2007; Hughes et al., 2004; Smith et al., 2011; Wu et al., 2008). Different subunit composition is responsible for specific properties of different complexes. Set1a-Set1b complexes contain a subunit, Wdr82 (Lee and Skalnik, 2008; Wu et al., 2008), that mediates crosstalk between transcription-coupled histone H2B monoubiquitination and H3K4 trimethylation (Kim et al., 2009). Because of this mechanism, Set1a-Set1b complexes are recruited after transcriptional activation has initiated and therefore in general they have little impact on transcription. However, Set1a-Set1b complexes can also be recruited by a transcription-independent mechanism that relies on direct recognition of unmethylated CpG dinucleotides in CpG islands by the CXXC domain of the Cfp1 subunit (Thomson et al., 2010). MLL complexes may not be recruited by a transcription-dependent mechanism at all. In the case of MLL1 and MLL4, a CXXC domain in the MLL subunits themselves may be essential for binding unmethylated CpG dinucleotides and for recruitment to CpG islands. The MLL2 and MLL3 complexes, instead, contain subunits that mediate association with nuclear receptors (Cho et al., 2007).

Although MLL1 and MLL4 are produced from paralogous genes related to *Drosophila* Trithorax (Trx) and are part of identical complexes, they have both redundant and nonredundant functions. At Hox loci, Mll1 is required for H3K4 methylation of a small subset of genes. However, absence of menin, a component of MLL1 and MLL4 complexes (Hughes et al., 2004), results in near global loss of H3K4me3 at Hox loci, indicating redundancy between the two enzymes (Wang et al., 2009). Mouse phenotypes resulting from loss of Mll1 are invariably severe but differ depending on the mutant allele engineered in the mouse (Ayton et al., 2001; Yagi et al., 1998; Yu et al., 1995). Mll1 is required for definitive hematopoiesis, in part through maintenance of the expression of a subset of Hox genes (Ernst et al., 2004a, 2004b). Conversely, Mll4 has unique and nonredundant roles in controlling bulk H3K4me3 in oocytes (Andreu-Vieyra et al., 2010), and its loss in adults results in both male and female sterility (Glaser et al., 2009). Moreover, deletion of *Mll4* in utero before E10.5 is lethal and associated with widespread developmental and growth defects, suggesting a specific requirement for Mll4 in early development (Glaser et al., 2006, 2009). Consistent with the notion that MLL1 and MLL4 exert exquisitely timed roles during development, deletion of *Mll4* after E11.5 did not have any obvious phenotypic consequence (Glaser et al., 2009).

By using a combination of epigenomic and transcriptomic analyses in *Mll4* mutant mice, we found that Mll4 loss in mouse macrophages causes hyporesponsiveness to lipopolysaccharide (LPS). A mechanistic dissection of the phenotype uncovered a specific underlying defect, namely the absence of GPI-anchored proteins on the cell surface. The glycosylphosphatidylinositol (GPI) anchor is a glycolipidic structure composed of a linear glycan containing phosphoethanolamine (PE), three mannose residues (MR), and a nonacetylated glucosamine (GlcN) linked to phosphatidylinositol (PI) (Kinoshita et al., 2008). The PI moiety contains two saturated fatty acid chains critical for association with membrane microdomains. GPI anchor precursors are synthesized in the endoplasmic reticulum through nine sequential steps and attached to the C termini of proteins bearing a GPI-attachment signal (Kinoshita et al., 2008). The first step of GPI biosynthesis is controlled by the GPI-GlcNAc transferase complex (GPI-GnT), which consists of eight distinct proteins. We found that the expression of one essential component of this enzyme, Pigp (Watanabe et al., 2000), requires Mll4-mediated antisilencing. Defective GPI anchor synthesis in *Mll4* mutant macrophages caused loss of membrane association of CD14, a glycoprotein retained on the surface of myelomonocytic cells via a GPI anchor. CD14 is involved in recognition of microbial molecules, most notably LPS (Wright et al., 1990), which are then transferred to the corresponding Toll-like receptor (TLR) to trigger downstream signaling events. The role of CD14 is therefore to enhance sensitivity of innate immune cells to LPS and other TLR agonists (Haziot et al., 1996; Lee et al., 1992). In fact, lack of membrane-anchored CD14 in $Mll4^{-/-}$ macrophages globally impaired the LPS response. Thus, through the control of GPI-anchor synthesis, Mll4 enables optimal responsiveness of macrophages to microbial stimuli.

RESULTS

Gene-Selective H3K4me3 Loss in $Wbp7^{-/-}$ Macrophages

To delete *Wbp7* in adult mice, we used a floxed *Wbp7* allele based on the "knock-out first strategy" (Testa et al., 2004) in which exon 2 is flanked by loxP sites (Glaser et al., 2006). $Wbp7^{fl/fl}$ mice were crossed to Rosa26-CreERT2 heterozygous mice to induce Cre-mediated recombination upon in vivo administration (by gavage feeding) of tamoxifen. Recombination results in a frame-shifted transcript carrying a premature stop codon (Glaser et al., 2006). Detection of the genomic recombination product and analysis of exon 2 containing transcripts by qRT-PCR indicated that recombination is both very efficient and virtually complete (Figure S1A). Hereinafter, mice and cells generated from Cre-mediated recombination of the floxed *Wbp7* allele will be indicated as $Wbp7^{-/-}$. Throughout the study, $Wbp7^{+/-}$ macrophages harboring the Rosa26-CreERT2 allele were used as control.

Macrophages generated in vitro from $Wbp7^{-/-}$ bone marrows were indistinguishable from $Wbp7^{+/-}$ macrophages (Figures S1B and S1C), indicating that Wbp7 is not required for their differentiation.

H3K4me3 profiles were analyzed in $Wbp7^{-/-}$ versus $Wbp7^{+/-}$ macrophages with chromatin immunoprecipitation (ChIP) coupled to high-throughput sequencing (ChIP-Seq) (Barski et al., 2007; Mikkelsen et al., 2007). Data were obtained both in untreated (UT) and LPS-stimulated (4 hr) macrophages. LPS is the prototypical microbial molecule triggering the deployment of an inflammatory gene expression program through a specific surface receptor, Toll-like receptor 4 (TLR4), which signals through multiple signaling pathways controlling the activation of several transcription factors (NF-κB, Irf3, AP-1, etc.) (Lee and Kim, 2007). Overall, deletion of *Wbp7* abrogated or reduced a substantial fraction of H3K4me3 peaks in both untreated

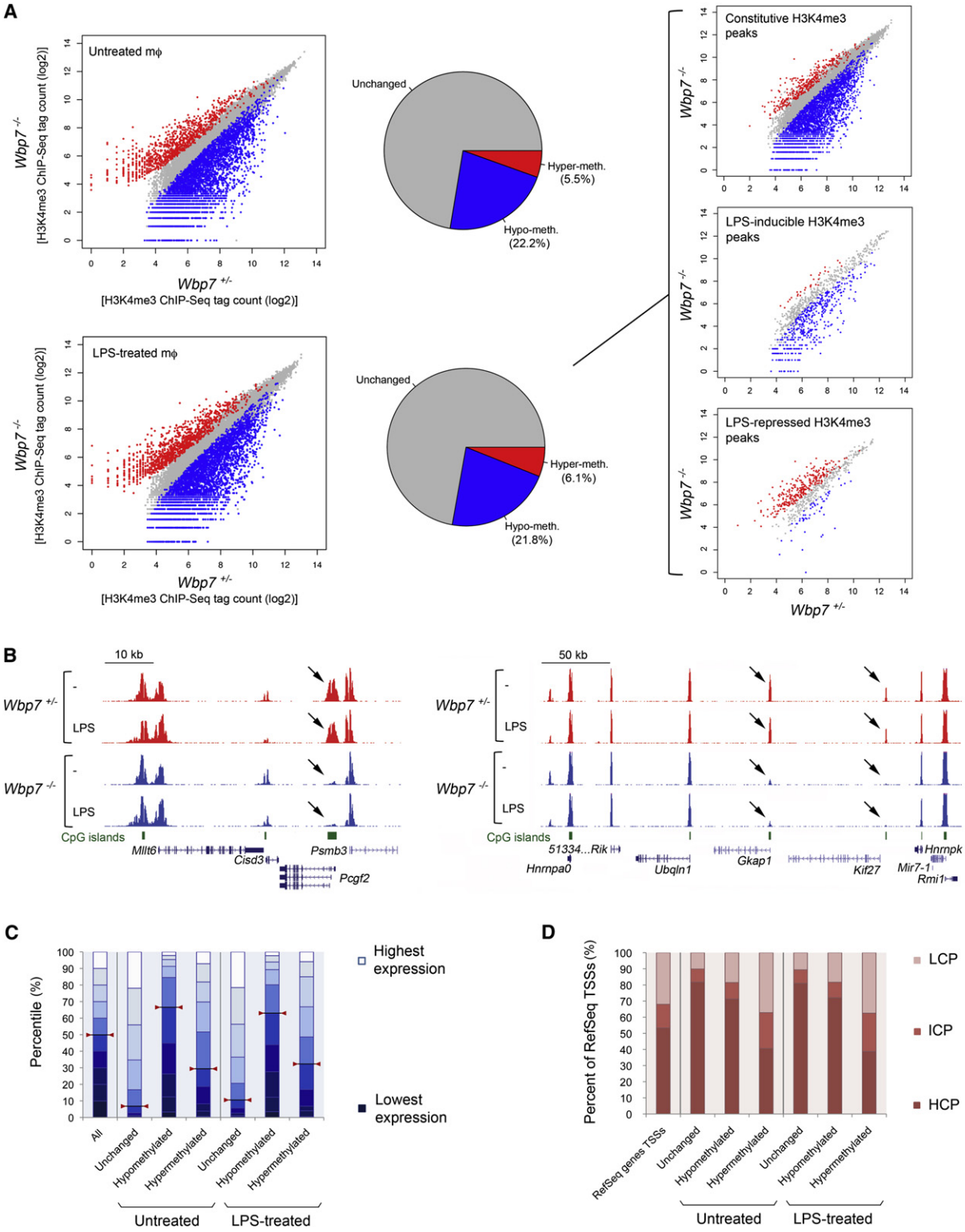

Figure 1. Gene-Selective H3K4me3 Loss in Wbp7-Deficient Macrophages

(A) Scatter plot showing H3K4me3 levels in *Wbp7*$^{-/-}$ and *Wbp7*$^{+/-}$ untreated (top) or LPS-treated (bottom) macrophages, as detected by ChIP-Seq. The pie charts in the middle indicate the fraction of H3K4me3 peaks that were either hypomethylated (blue) or hypermethylated (red) in *Wbp7*$^{-/-}$ macrophages. Scatter plots on the right show H3K4me3 peaks detected in LPS-stimulated cells at 4 hr and divided in constitutive, LPS-inducible, and LPS-repressed peaks.

(B) Two representative genomic regions are shown, in which Wbp7 loss caused H3K4me3 hypomethylation at selected peaks (arrows).

(22.2%, corresponding to 3,948 out of 17,824 total peaks at $p < 10^{-5}$) and LPS-treated (21.8%; 3,896/17,899) macrophages (Figure 1A, left; Table S1). By using a completely unrelated biological replicate (data not shown), overlap of hypomethylation was 88% at $p < 10^{-20}$ and 77.9% at $p < 10^{-5}$. We also detected low-magnitude increases in H3K4me3 at 5.5% of peaks in untreated macrophages and 6.1% in LPS-treated macrophages, probably reflecting secondary effects of Wbp7 loss. The dominance of H3K4me3 losses over H3K4me3 gains is indicated by the asymmetry of the scatter plots in Figure 1A. H3K4me3 is induced at a few hundred LPS-activated genes in macrophages (De Santa et al., 2009; Foster et al., 2007). By distinguishing constitutive from LPS-inducible H3K4me3 peaks, it became clear that Wbp7 affected both groups to a similar extent (Figure 1A, top and middle scatter plots on the right), even though most high-magnitude hypomethylations (those closer to the bottom-right corner of the plot) were detected in unstimulated cells. Intriguingly, H3K4me3 peaks that were diminished upon LPS stimulation in *Wbp7*$^{+/-}$ cells were conversely increased in *Wbp7*$^{-/-}$ macrophages (Figure 1A, bottom scatter plot on the right). As documented below, this apparently paradoxical result is readily explainable as an indirect effect. Representative genomic snapshots are shown in Figure 1B.

Overall, Wbp7 was required to maintain H3K4me3 levels at about one-fifth of genes in mouse macrophages, with a preference for moderately expressed genes containing CpG islands. First, gene expression (obtained from cDNA microarray data) was correlated to the status of hypo-, hyper-, or unchanged methylation according to H3K4me3 levels at the TSS (±2.5 kbp) in *Wbp7*$^{-/-}$ versus *Wbp7*$^{+/-}$ cells. The hypomethylated gene group showed a moderate enrichment of genes with intermediate expression and a strong underrepresentation of highly expressed genes ($p < 1 \times 10^{-15}$ in a chi-square test) (Figure 1C). Second high-CpG-content promoters were moderately overrepresented among the RefSeq genes showing hypomethylation in *Wbp7*$^{-/-}$, suggesting that CpG islands may represent preferential Wbp7 targets ($p < 1 \times 10^{-15}$ in a chi-square test) (Figure 1D). However, it is clear that differential CpG content does not suffice as a satisfactory explanation for the selectivity of the effects of Wbp7 deletion. We therefore searched for transcription factor (TF) binding sites overrepresented in the different groups. Although we could not identify any TF binding sites strongly enriched in hypomethylated genes, the group of genes showing no H3K4me3 changes in *Wbp7*$^{-/-}$ macrophages was instead characterized by a strong overrepresentation of multiple Ets family TF binding sites (Table S2 and Figure S1D). These data suggest that distinct compositions in TF binding sites may in fact underlie selective coupling of individual promoters to specific MLL proteins and that Ets TFs are uncoupled from Wbp7 in macrophages (or compensate for its loss). When the analyses reported in Figures 1C and 1D were repeated with a more restrictive threshold for the identification of hypomethylated peaks ($p < 10^{-10}$, see Supplemental Experimental Procedures), the conclusions were fully consistent with those reported above.

Finally, when the four Hox genes clusters were analyzed, small H3K4me3 changes were observed only at *Hoxa4* (Figure S1E). This result is consistent with the already described redundancy between Mll1 and Wbp7 at these loci (Wang et al., 2009).

Wbp7 Loss Attenuates the LPS Response

We measured gene expression changes induced by *Wbp7* deletion in unstimulated and LPS-stimulated macrophages by using cDNA microarrays. Considering a fold change of 1.5 and a $p < 0.01$ (for a biological triplicate), we found that 211 genes were downregulated by *Wbp7* deletion in unstimulated cells, about four times more than those that were upregulated (Figures 2A and 2B; Table S3), a result in line with the expected activating role of Wbp7. The total number of deregulated genes in *Wbp7*$^{-/-}$ macrophages was strongly increased upon LPS stimulation, providing an initial indication that Wbp7 loss has a higher impact on the transcriptional response to LPS than on basal transcription.

In line with previous reports (Guenther et al., 2007), there was a clear correlation between H3K4me3 loss and reduction in gene expression. Genes showing the strongest downregulation in *Wbp7*$^{-/-}$ cells were also those with the most significant hypomethylation (Figure 2C). Symmetrically, genes whose TSS showed the greatest hypomethylation were more likely to display reduced expression in the knockout (Figure 2D). However, more than 90% of hypomethylated genes didn't display reduced expression in *Wbp7*$^{-/-}$ macrophages (Tables S3 and S4).

A gene set enrichment analysis (GSEA) (Subramanian et al., 2005) provided evidence for a general defect in the LPS response in *Wbp7*$^{-/-}$ cells. We considered a total of four gene sets that included the genes downregulated or upregulated in *Wbp7*$^{-/-}$ as compared to *Wbp7*$^{+/-}$ macrophages at 2 hr (Figure 2E) or 4 hr (Figure 2F) of LPS stimulation. All RefSeq genes were ranked (*x* axis) according to their relative level of expression in control (*Wbp7*$^{+/-}$) macrophages treated with LPS for 2 hr (Figure 2E) or 4 hr (Figure 2F) as compared to untreated macrophages. The distribution of the four gene set components relative to their respective ranked lists indicated that genes downregulated in LPS-treated *Wbp7*$^{-/-}$ macrophages were overrepresented among those induced by LPS treatment. Conversely, genes upregulated in *Wbp7*$^{-/-}$ macrophages were overrepresented among those downregulated by LPS treatment (FDR < 0.01 in permutation tests). In other words, genes whose expression was upregulated by LPS were less upregulated in the absence of Wbp7, and genes whose expression was downregulated in response to LPS stimulation were less downregulated in Wbp7 mutants. Hence, Wbp7 loss attenuated the transcriptional response to LPS that affected in a similar manner the genes induced and those repressed in response to stimulation. Consistent conclusions were obtained with a fold change of 2 and a $p < 0.01$ as thresholds (Figure S2).

(C) Genes were divided in ten groups based on their expression level in unstimulated conditions (via the microarrays described in this study). Bar graph shows the distribution of all genes (left) or the genes where loss of Wbp7 caused no changes in H3K4me3, hypomethylation or hypermethylation, respectively, in unstimulated or stimulated conditions.

(D) Bar graph showing the distribution of high-, intermediate-, or low-density CpG promoters (HCP, ICP, and LCP) for all genes (left) or genes classified as unchanged, hypomethylated, or hypermethylated in *Wbp7*$^{-/-}$ macrophages.

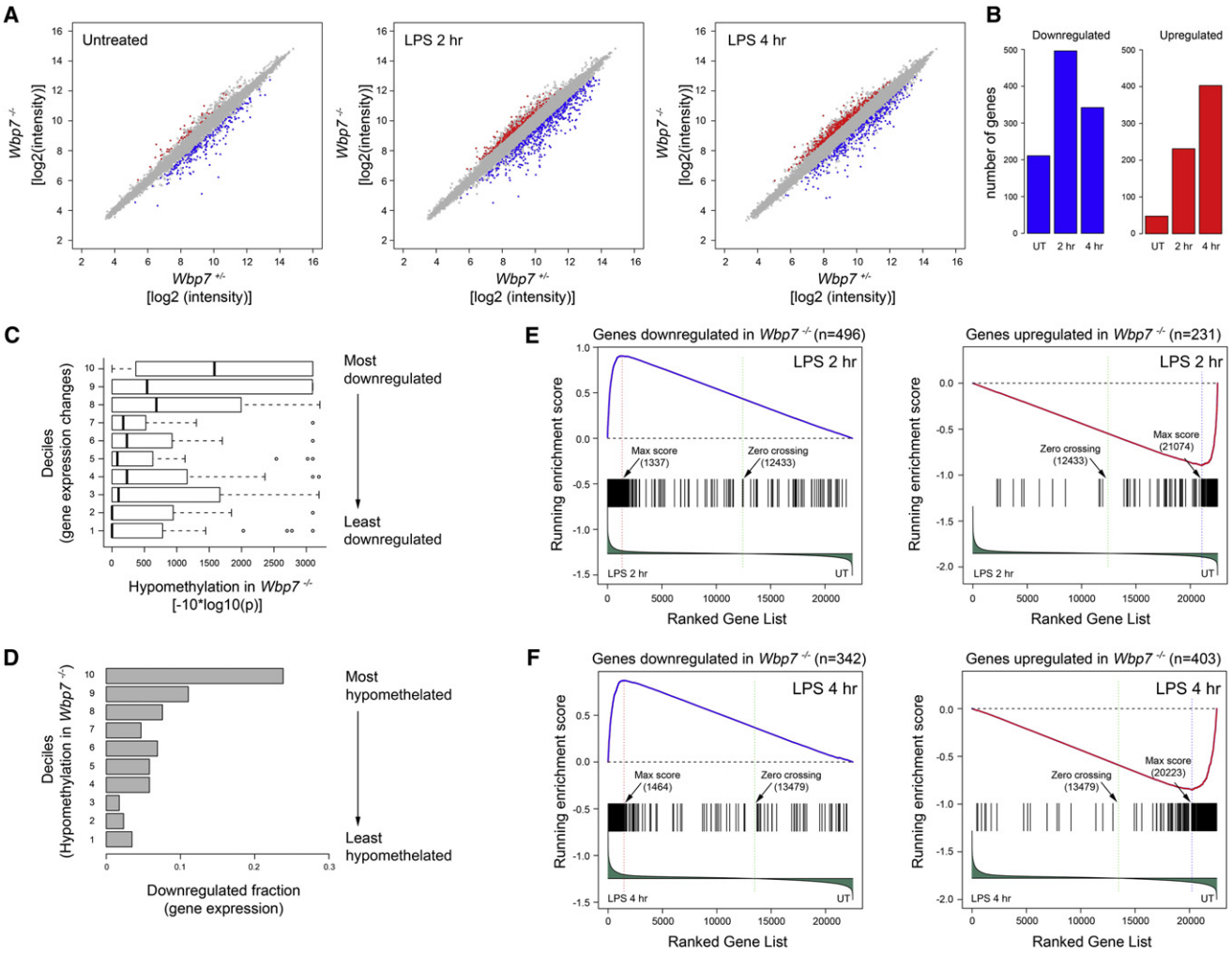

Figure 2. Widespread Attenuation of LPS-Induced Gene Expression Changes in *Wbp7*$^{-/-}$ Macrophages

(A) Scatter plot showing gene expression changes in unstimulated and LPS-stimulated *Wbp7*$^{-/-}$ macrophages as compared to control cells. Downregulated genes are indicated in blue, upregulated genes in red.

(B) Bar graph showing the actual number of downregulated or upregulated genes in *Wbp7*$^{-/-}$ macrophages (fold change 1.5; $p < 0.01$).

(C) Bar plot showing the correlation between reduction in gene expression (*y* axis) and H3K4me3 hypomethylation (*x* axis) in *Wbp7*$^{-/-}$ macrophages. Downregulated transcripts were ranked according to their fold change, from the most to the least downregulated in *Wbp7*$^{-/-}$ compared to control macrophages. Transcripts were then split into deciles and for each decile the level of hypomethylation (expressed as the distribution of -10*log10(p value) obtained from MACS) was computed and shown in the box plots.

(D) The reciprocal correlation between hypomethylation and reduction in gene expression is shown. Genes with hypomethylated TSS were ranked from the most to the least statistically significant (*y* axis). Then they were split into deciles and for each decile the fraction of downregulated genes (*x* axis) was computed.

(E and F) GSEA in *Wbp7*$^{-/-}$ macrophages stimulated with LPS for 2 hr (E) or 4 hr (F). The genes in the lists were sorted (from left to right) based on their relative level of expression in LPS-stimulated versus untreated control macrophages.

Transcriptional Impairment versus H3K4me3 Changes at LPS-Inducible Genes

To obtain further insight into the transcriptional phenotype of *Wbp7*$^{-/-}$ macrophages, we analyzed a selected panel of LPS-induced genes with well-characterized properties by quantitative RT-PCR.

Nfkbia, which encodes the NF-κB inhibitory subunit IkBα, is a primary LPS response gene whose transcriptional activity directly reflects nuclear NF-κB levels (Giorgetti et al., 2010). Therefore, *Nfkbia* mRNA induction in response to LPS stimulation provides a direct readout of NF-κB activity. In *Wbp7*$^{-/-}$ macrophages, *Nfkbia* mRNA induction was reduced over control cells at all time points examined (Figure 3), indicating a defective NF-κB activation. Importantly, H3K4me3 levels at *Nfkbia* were identical in knockout and control cells (Figure 3, right) suggesting that loss of Wbp7 had an H3K4me3-independent effect on *Nfkbia* expression. Similarly, the induction of other primary response genes regulated mainly by NF-κB-like *Cxcl1*, *Cxcl2*, and *Nfkbiz* was also impaired in *Wbp7*$^{-/-}$ macrophages (Figure 3). However, their promoters showed no or minimal H3K4me3 changes. We also examined one late primary response gene, *Ccl5*, and one secondary response gene, *Il6*, with

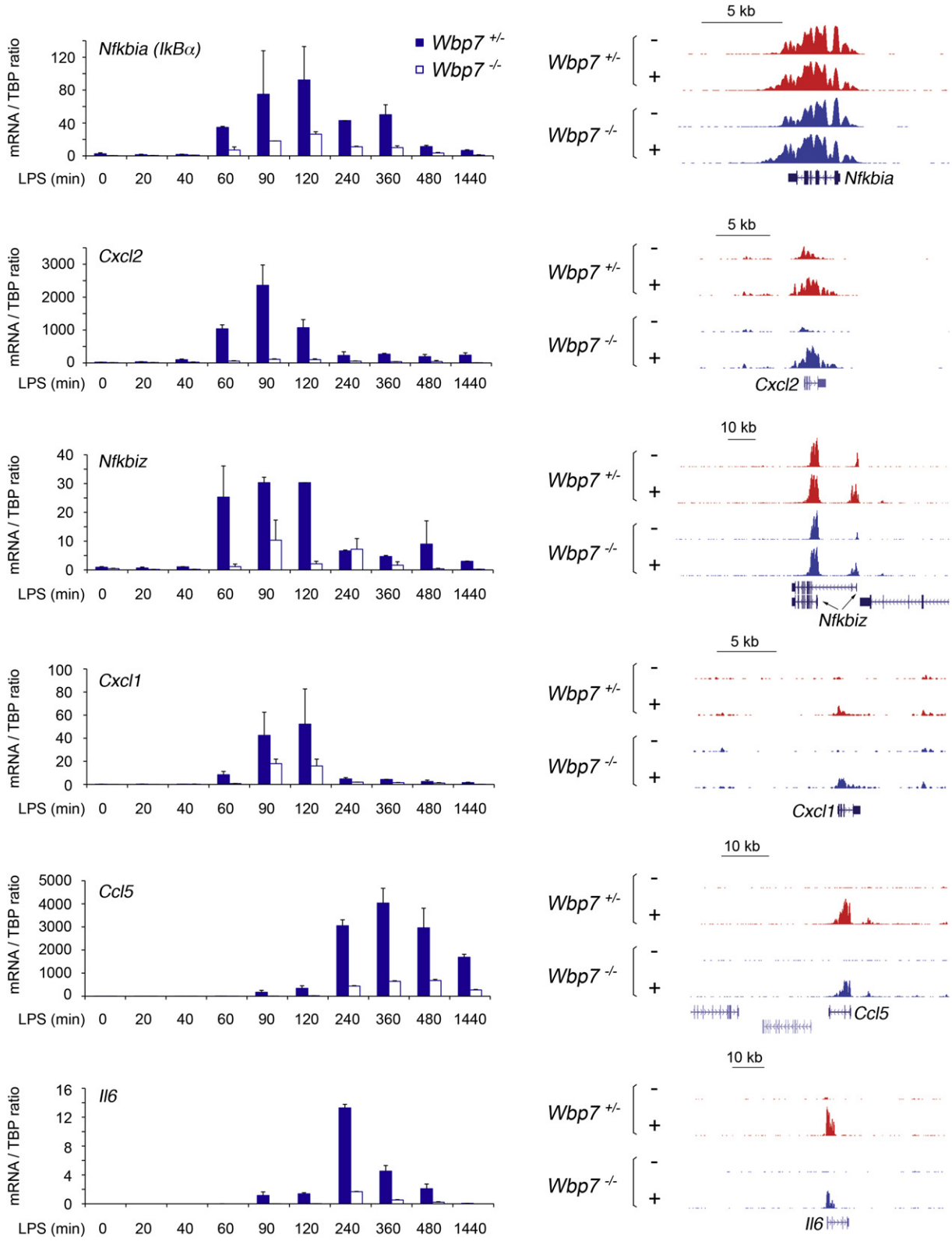

Figure 3. Transcriptional Impairment versus H3K4me3 Levels at Canonical Inflammatory Genes

Relative mRNA levels of the indicated genes were measured with qRT-PCR in control and *Wbp7*$^{-/-}$ macrophages stimulated with LPS as indicated. mRNA levels were normalized to TBP (error bars: SD). The genomic snapshots in the right panels indicate H3K4me3 levels at the same genes in control and knockout macrophages, before and after (4 hr) LPS stimulation.

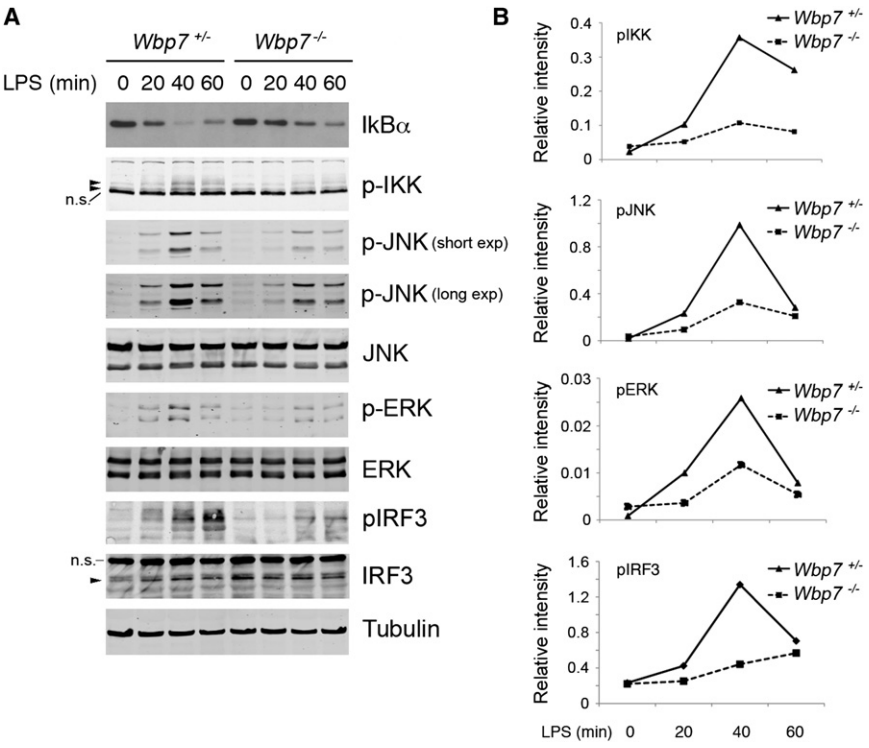

Figure 4. LPS-Triggered Signaling Events in Macrophages Lacking Wbp7

(A) Protein immunoblots were carried out with the indicated antibodies on cytosolic lysates of control and *Wbp7*$^{-/-}$ macrophages stimulated with LPS as indicated. Images were acquired with a Li-Cor Odyssey imaging system. Arrowheads, phospho-IKK; n.s., nonspecific band. For JNK, ERK, and IRF3, protein immunoblots are shown with both a phospho-specific antibody (p-JNK, p-ERK, and p-IRF3) and an antibody recognizing the proteins irrespective of phosphorylation. Tubulin: loading control.

(B) Digital quantification (normalized for the respective control) for some of the images.

a complex (and therefore more fragile) regulation reflecting the convergence of multiple signaling pathways. Also at these genes Wbp7 loss caused a strong, albeit incomplete, transcriptional impairment without any strong reduction in H3K4me3 levels (Figure 3). Altogether, we conclude that loss of Wbp7 impairs the induction of inflammatory genes in a manner that is not directly related to the deposition of H3K4me3 at these genes.

Consistent with these data, we found that de novo H3K4 trimethylation induced by LPS at genes like *Il6* and *Ccl5* (and at nearly all other genes where this mark was induced by stimulation) was entirely dependent on Set1a-Set1b and that it could be completely ablated without significantly affecting mRNA levels (data not shown). Finally, when using agonists of TLRs other than TLR4, transcriptional responses were similarly impaired (Figure S3).

A Signaling Defect in *Wbp7*$^{-/-}$ Macrophages

Two major clues pointed to a signaling defect in *Wbp7*$^{-/-}$ macrophages. First, GSEA showed a global attenuation of the transcriptional response to LPS that similarly impacted induced and repressed genes. Second, impaired *Nfkbia* mRNA induction suggested a reduced NF-κB activation and/or nuclear import in response to LPS stimulation. Therefore, we analyzed the activation of LPS-inducible signaling pathways in *Wbp7*$^{-/-}$ versus *Wbp7*$^{+/-}$ macrophages. Phosphorylation of the IκB kinases (IKK) was reduced several fold in *Wbp7*$^{-/-}$ cells (Figures 4A and 4B). Consistent with this result, although in control cells degradation of IκBα was complete at 40 min and initial resynthesis (which is NF-κB dependent) was already observed at 60 min, in *Wbp7*$^{-/-}$ macrophages the whole process of degradation and resynthesis was delayed and impaired (Figure 4A). Impaired signaling in *Wbp7*$^{-/-}$ cells was not restricted to the IKK/NF-κB pathway. Indeed, activation of extracellular signal-regulated kinases (Erk1 and Erk2) and c-Jun N-terminal kinases (JNK1 and JNK2) were also reduced in mutant cells (Figures 4A and 4B). Most importantly, TLR4-induced phosphorylation of the transcription factor IRF3, which requires the adaptor TRIF and is essential for the activation of the interferon beta (*Ifnb1*) gene, was severely reduced in Wbp7-deficient cells. Consistent with this result, LPS induction of the *Ifnb1* mRNA was almost completely abolished in *Wbp7*$^{-/-}$ macrophages (Figure S4). Overall, *Wbp7*$^{-/-}$ macrophages displayed a general signaling defect in response to LPS stimulation.

Transcription and H3K4me3 Levels of Pigp Require Wbp7

To determine the mechanistic basis for impaired signaling in Wbp7 knockout macrophages, we inspected the list of the genes most affected by *Wbp7* deletion. Notably, this list includes *Magohb*, the only gene whose expression is completely dependent on Wbp7 in embryonic stem cells (Glaser et al., 2009), thereby suggesting that some Wbp7 targets may be shared across cell types.

Two genes were strongly downregulated in unstimulated *Wbp7*$^{-/-}$ macrophages: *Pigp* and *Taf9b* (Figure 5A). The latter is a paralog of Taf9, a general transcription factor that binds to an RNA polymerase II core promoter element, the DPE (downstream core promoter element) (Frontini et al., 2005). Although the specific role of Taf9b in relation to Taf9 is still incompletely defined, it may be involved in bringing about some of the transcriptional consequences of Wbp7 deletion.

Pigp was the main candidate to account for the signaling deficiency we observed in *Wbp7*$^{-/-}$ cells. Pigp is an essential component of the GPI-GlcNAc transferase (Watanabe et al., 2000), the enzyme that controls the first and rate-limiting step in GPI anchor synthesis (Kinoshita et al., 2008). Because CD14, which enhances responsiveness of TLR4 to LPS (Lee et al., 1992), is a GPI-anchored protein, we hypothesized that the loss of GPI anchor synthesis and the consequent loss of membrane-bound CD14 may underlie the signaling impairment of *Wbp7*$^{-/-}$ macrophages.

A

Gene Symbol	mRNA ($Wbp7^{-/-}$ vs. $Wbp7^{+/-}$)	H3K4me3 ($Wbp7^{-/-}$ vs. $Wbp7^{+/-}$)	H3K27me3 ($Wbp7^{-/-}$ vs. $Wbp7^{+/-}$)	CpG
Pigp	-17,83	0,028	31,77	HCP
Taf9b	-16,64	0,014	4,9	HCP
Stau2	-6,5	0,014	ND	-
Maged1	-6,2	0,036	3,51	HCP
Dip2c	-5,21	0,079	ND	HCP
Fmnl2	-5,05	0,101	6,07	HCP
Magohb	-4,84	0,011	1,87	HCP
Pde3b	-4,81	0,148	1,04	HCP
Arhgap5	-4,5	0,211	52,77	LCP
Slc30a4	-4,4	0,069	2,2	HCP

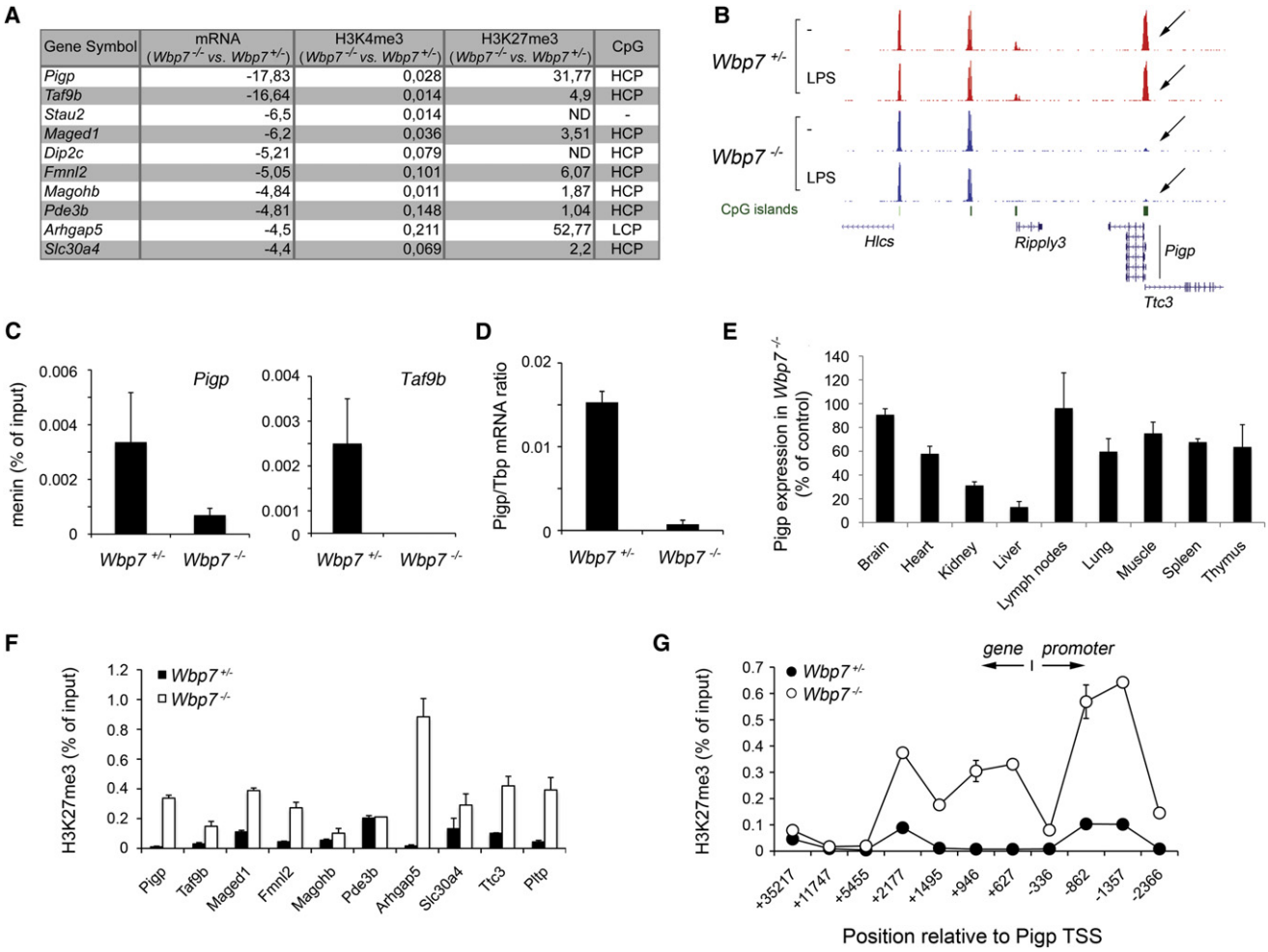

Figure 5. Transcriptional and Epigenomic Changes at the *Pigp* Gene in Macrophages Lacking Wbp7

(A) Table showing the top downregulated genes in unstimulated $Wbp7^{-/-}$ macrophages and their H3K4me3 and H3K27me3 levels measured by ChIP-QPCR. ND, not determined.

(B) Genomic snapshot showing H3K4me3 loss at *Pigp*. *Pigp* transcript variants are indicated.

(C) Anti-menin ChIP in control and $Wbp7^{-/-}$ cells. Immunoprecipitated DNA was amplified with primers spanning the Pigp (left) and the Taf9b (right) promoters.

(D) qRT-PCR showing loss of *Pigp* expression in $Wbp7^{-/-}$ macrophages (error bars: SD).

(E) *Pigp* mRNA was quantified in different tissues from $Wbp7^{+/-}$ and $Wbp7^{-/-}$ mice. TBP-normalized data are expressed as percent of control.

(F) H3K27me3 ChIP-QPCR. H3K27me3 was measured at the promoters of a representative set of genes downregulated in $Wbp7^{-/-}$ macrophages (error bars: SD).

(G) H3K27me3 levels over the *Pigp* gene locus. H3K27me3 was measured by ChIP-QPCR. Primers positions are relative to the TSS of *Pigp*.

To evaluate this hypothesis, we first inspected H3K4me3 levels at the *Pigp* TSS and found that the modification is nearly completely absent in $Wbp7^{-/-}$ macrophages, with residual levels lower than 3% of control cells (Figures 5A and 5B). Second, anti-menin ChIP in wild-type and $Wbp7^{-/-}$ cells confirmed that *Pigp* is a bona fide Wbp7 target (Figure 5C). Third, we confirmed by quantitative RT-PCR that *Pigp* expression is abrogated in $Wbp7^{-/-}$ cells (Figure 5D). Analysis of multiple tissues from $Wbp7^{-/-}$ mice (Figures 5E and S5A) demonstrated a strong contribution of Wbp7 to *Pigp* expression in liver and kidney, whereas other tissues or organs in which CreER is highly efficient (e.g., muscle and spleen) were only marginally affected (the brain was used as a negative control because Rosa26-CreERT2 achieves only partial Wbp7 deletion in the central nervous system).

Because H3K4me3 may have an antisilencing role and specifically prevent H3K27me3 deposition (Klymenko and Müller, 2004), we also analyzed H3K27me3 levels at *Pigp* and at other genes dependent on Wbp7 for their expression. Although H3K27me3 was negligible at the *Pigp* gene promoter in control cells, it was greatly increased in the absence of Wbp7 (Figures 5A and 5F), spreading over about 8 kilobases including promoter and gene body, while leaving adjacent genes unaffected (Figure 5G). Several other Wbp7-dependent genes containing a CpG island (such as *Taf9b*, *Maged1*, *Magohb*) also showed increased H3K27me3 (Figure 5F). H3K4me3 at the Pigp

promoter was unaffected by LPS activation of wild-type macrophages (Figure S5B); however, promoter acetylation and mRNA levels were moderately reduced upon sustained stimulation (Figures S5C and S5D).

Global Loss of GPI-Anchored Proteins and Membrane-Bound CD14 in *Wbp7*$^{-/-}$ Macrophages

Because Pigp is essential for the activity of the 8-subunit GPI-GlcNAc transferase complex, the enzyme catalyzing the first step of GPI anchor synthesis (Watanabe et al., 2000), we analyzed surface expression of GPI-anchored proteins in *Wbp7*$^{-/-}$ macrophages. To this aim, we exploited the ability of a bacterial toxin, aerolysin, to bind the GPI anchor with high affinity (Diep et al., 1998). A fluorescently labeled inactive aerolysin precursor (FLAER) is routinely used for diagnosis of paroxysmal nocturnal hemoglobinuria, in which lack of Piga (another component of the GPI-GlcNAc transferase) results in loss of GPI-anchored proteins on erythrocytes (Brodsky et al., 2000).

FLAER staining was stable during a prolonged LPS stimulation of WT macrophages (Figure S5E), suggesting that the moderate reduction in Pigp mRNA levels observed in these conditions (Figure S5D) is not sufficient to affect the GPI anchor synthesis capacity of macrophages. Conversely, flow cytometry analysis demonstrated a nearly complete absence of FLAER staining in *Wbp7*$^{-/-}$ macrophages (Figure 6A), thus revealing a global reduction of GPI-anchored proteins on the cell surface. In keeping with this result, staining of CD14, a GPI-anchored protein, was almost completely lost in *Wbp7*$^{-/-}$ macrophages (Figure 6A). Another GPI-anchored protein tested, uPAR, similarly showed strongly reduced surface staining in *Wbp7*$^{-/-}$ macrophages (Figure 6A).

CD14 mRNA was unaffected by *Wbp7* deletion, indicating that loss of surface staining is not due to a transcriptional effect of Wbp7 loss (Figure 6B). Similarly, TLR4 mRNA was not altered by Wbp7 loss (Figure 6B) and its surface expression was unaffected (Figure S6).

CD14 captures LPS and transfers it to TLR4, thus facilitating TLR4 triggering and downstream signaling at low agonist concentrations (Haziot et al., 1996; Lee et al., 1992). If the impairment in LPS-regulated gene expression in *Wbp7*$^{-/-}$ macrophages is mainly due to a CD14-linked defect in signaling, a simple prediction is that the defect should be partially rescued by increasing LPS concentration. In keeping with this prediction, a 10-fold increase in LPS concentration rescued or attenuated the gene expression defect at several genes tested (Figure 6C). In some cases gene induction at the maximal LPS concentration was even higher than in control cells, reflecting a role of CD14 in postinduction TLR4 downregulation (Zanoni et al., 2011).

Restoring Membrane CD14 Rescues the Transcriptional Defects

To determine whether Pigp re-expression in *Wbp7*$^{-/-}$ macrophages is sufficient to rescue the transcriptional phenotype, we infected *Wbp7*$^{-/-}$ macrophages with a retrovirus expressing the Pigp cDNA. Flow cytometry analysis showed that Pigp expression in *Wbp7*$^{-/-}$ cells restored surface levels of CD14 similar to those of wild-type cells (Figure 7A). Strikingly, induction of genes that are strongly dependent on Wbp7 for maximal expression was rescued in Pigp reconstituted cells (Figure 7B). We also reconstituted surface CD14 by retroviral transduction of CD14 fused to the transmembrane domain of mouse TLR4 (Figure 7C). Also in this case, defective LPS induction of inducible genes could be rescued to wild-type levels (Figure 7D).

Overall, these data demonstrated a central role for loss of GPI-anchored CD14 in the impaired response of Wbp7-deficient macrophages to LPS.

DISCUSSION

In this study, we identified a specific role for Wbp7 in the synthesis of GPI anchors in macrophages. This role of Wbp7 is exercised through the tight transcriptional control of a single gene, *Pigp*, encoding an essential component of the enzymatic complex that catalyzes the first step of GPI-anchor synthesis. GPI anchors are indirectly implicated in microbial recognition, as shown by the fact that CD14, which enhances detection of LPS (Wright et al., 1990) and other microbial molecules (Baumann et al., 2010; Lee et al., 2006a) through transfer to the competent TLRs, requires a GPI anchor for membrane loading. Moreover, CD14 itself may deliver activation signals (despite the lack of a cytoplasmic tail), as demonstrated by its requirement for TLR4-independent, LPS-induced NFAT activation in dendritic cells (Zanoni et al., 2009). Whereas membrane anchoring of CD14 appears to represent a particularly relevant aspect of GPI anchor biosynthesis in macrophages, it is likely that loss of GPI anchors will affect localization and function of many other biologically relevant proteins in this system, such as the urokinase plasminogen activator receptor (uPAR), which regulates the proteolytic activity of the uPA serine protease (Blasi and Sidenius, 2010).

Lack of membrane-associated CD14 and the ensuing defect in LPS recognition resulted in a straightforward cascade of effects: (1) a reduced activation of intracellular signaling pathways, including the IKK-NF-κB pathway, the MAPK pathways, and the TRIF/IRF3 pathway, followed by (2) a broad attenuation of both positive and negative gene expression changes triggered by LPS. The transcriptional defects were partially rescued simply by increasing LPS concentration, a result consistent with the central role of CD14 in this phenotype. More directly, re-expression of Pigp or membrane-anchored CD14 in *Wbp7*$^{-/-}$ cells reverted the transcriptional defects.

The central role played in this phenotype by the impact of Wbp7 on signaling is underscored by the observation that Wbp7 loss attenuated not only LPS-induced increases in H3K4me3 (which may reflect a direct role of Wbp7 in de novo deposition of H3K4me3) but also LPS-induced reductions of this histone modification, which probably represent an indirect consequence of the signaling defect. Because of its requirement for GPI anchor synthesis and CD14 attachment to the macrophage membrane, Wbp7 can thus be considered as a component of the innate immune system in its own right.

The impact of Wbp7 loss on the macrophage epigenome was broad, with about 20% of active genes showing reduced H3K4me3 levels in mutant cells. Attempts to identify specific sequence features responsible for Wbp7 dependence of H3K4me3 failed to generate clear-cut results, even though hypomethylation tended to occur at high CpG-containing promoters and at moderately but not highly expressed genes. Moreover,

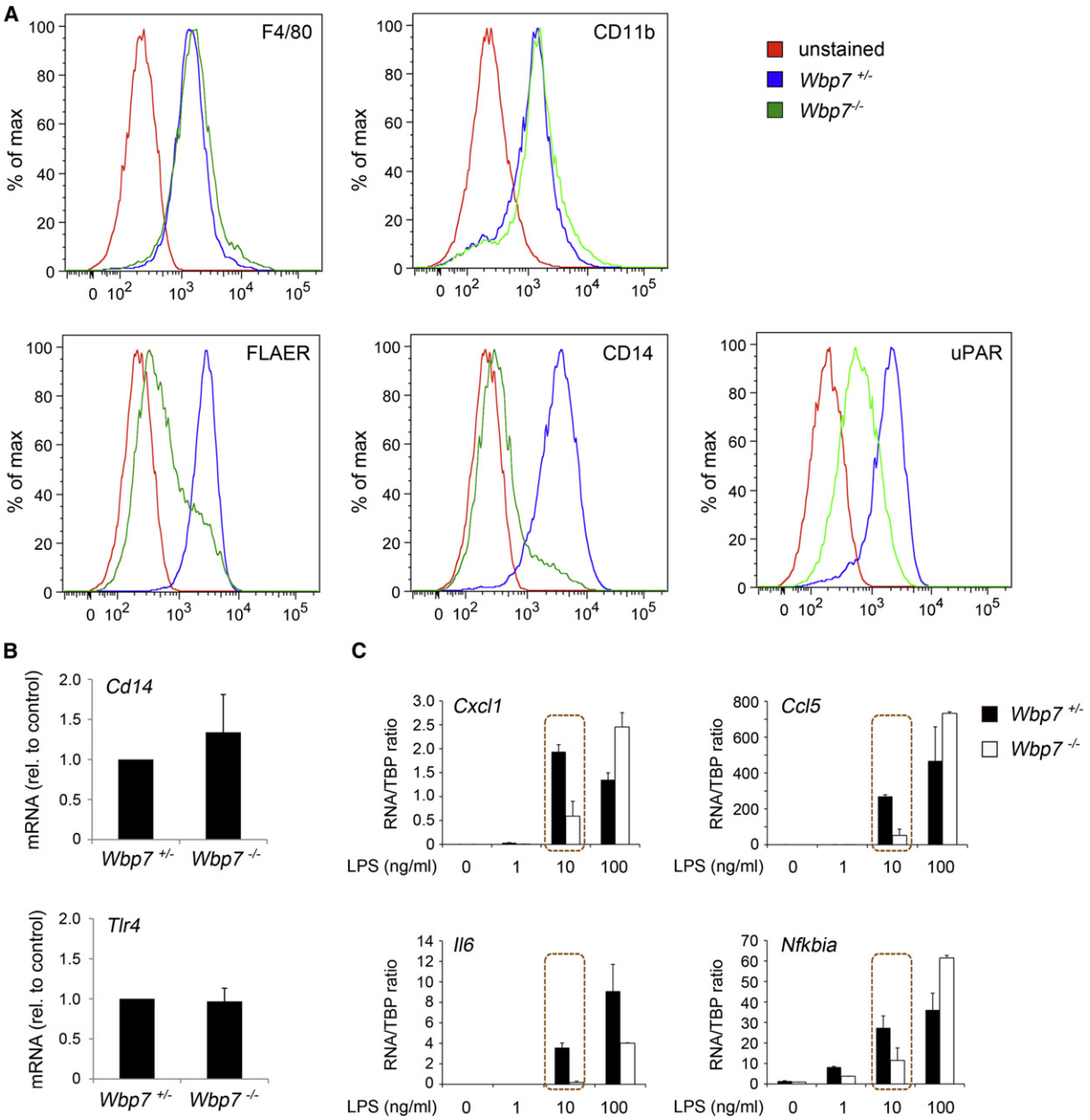

Figure 6. Global Loss of GPI-Anchored Proteins and Lack of Membrane-Associated CD14 in *Wbp7*$^{-/-}$ Macrophages

(A) FACS analysis on *Wbp7*$^{-/-}$ and control macrophages was carried out with antibodies against F4/80 (Emr1), Cd11b, CD14, and uPAR, and with fluorescent aerolysin (FLAER).

(B) mRNA levels for *Cd14* and *Tlr4* were measured by qRT-PCR in three independent biological replicates. Data obtained in *Wbp7*$^{-/-}$ macrophages are expressed relative to control macrophages (error bars: SEM).

(C) mRNA levels for the indicated genes were measured by quantitative RT-PCR in control or *Wbp7*$^{-/-}$ macrophages stimulated with the indicated concentrations of LPS. The dotted boxes indicate the LPS dose used elsewhere in this study (10 ng/ml). Error bars: SD.

when compared to hypomethylated genes, those showing no methylation changes in the knockout were enriched for Ets family TF binding sites, suggesting that TFs bound to promoters represent an important determinant of selectivity toward specific MLL proteins. In spite of the amplitude of epigenomic effects of Wbp7 loss, the number of bona fide Wbp7-dependent genes was very small, with only 6 genes showing more than a 5-fold and 30 genes more than a 3-fold reduction in expression in unstimulated *Wbp7*$^{-/-}$ macrophages. Overall, only 7.3% of the genes showing reduced H3K4me3 in Wbp7-deficient macrophages also showed reduced mRNA levels. This result suggests that in most cases reduced H3K4me3 in *Wbp7*$^{-/-}$ cells will not lead to detectable transcriptional effects. At least for some of the most downregulated genes, H3K4me3 reduction was

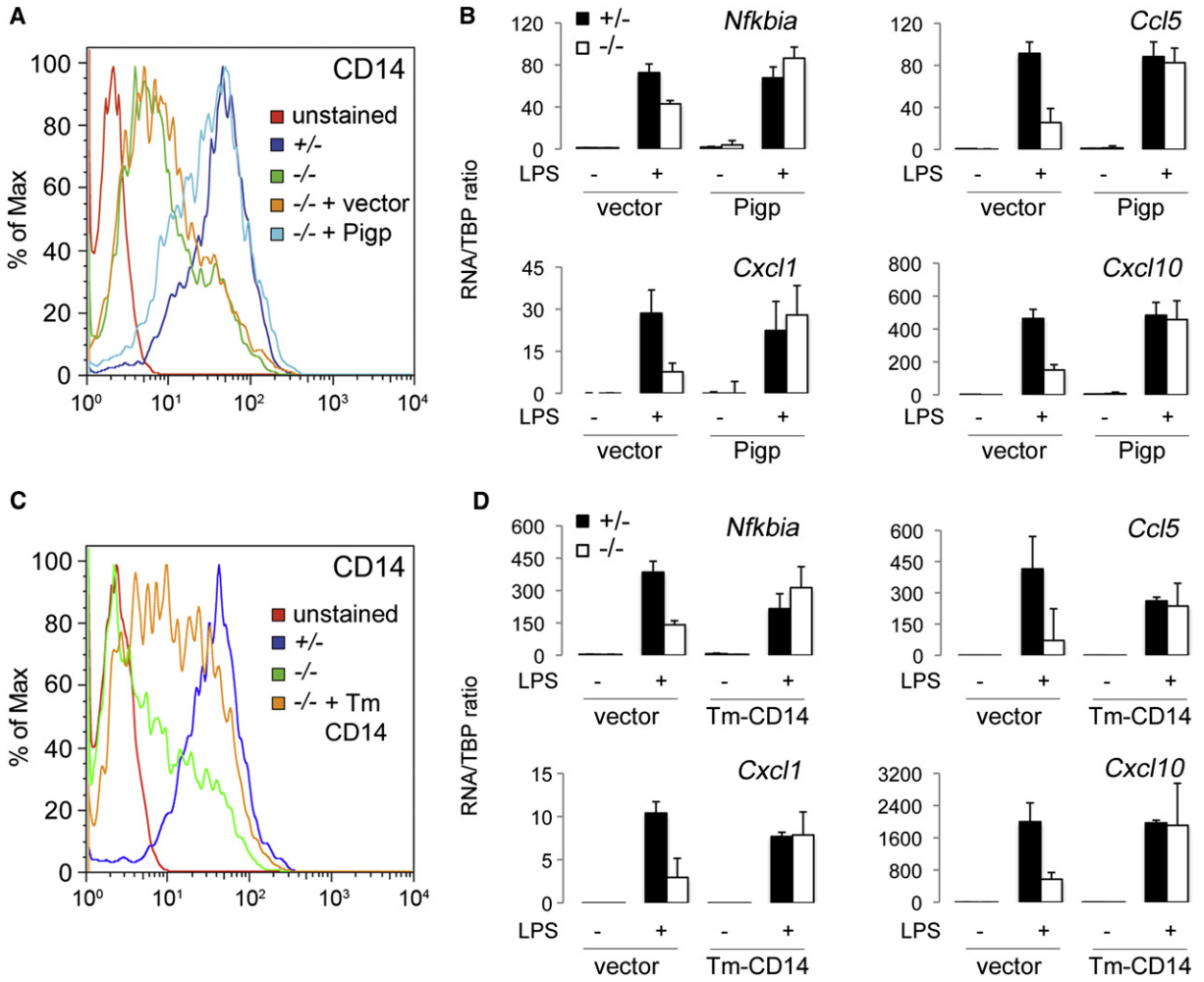

Figure 7. Rescue of Surface CD14 Restores Transcriptional Responses to LPS

(A) FACS analysis of surface CD14 in *Wbp7*$^{-/-}$ cells uninfected or infected with an empty virus (vector) or a Pigp-expressing virus.

(B) mRNA levels for the indicated LPS-inducible genes upon Pigp re-expression in *Wbp7*$^{-/-}$ cells (error bars: SD).

(C) Anti-CD14 FACS analysis in *Wbp7*$^{-/-}$ macrophages transduced with a retroviral vector expressing CD14 fused to the transmembrane domain of TLR4 (Tm-CD14).

(D) mRNA for the indicated genes were measured by quantitative RT-PCR in *Wbp7*$^{+/-}$ and *Wbp7*$^{-/-}$ macrophages transduced with either a control (vector) or a Tm-CD14-expressing retrovirus.

accompanied by an increase in H3K27me3, suggesting that Wbp7-deposited H3K4me3 has an antisilencing role, as demonstrated for MLLs orthologs in *Drosophila* (Klymenko and Müller, 2004) and Wbp7 in mouse embryonic stem cells (Glaser et al., 2009). Moreover, the gene most dependent on Wbp7 for expression, *Pigp*, was among those with the highest H3K27me3 enrichment.

These data became particularly meaningful in the conceptual frame of the standard models describing activity and biological role of chromatin modifiers. The general assumption is that most histone methyltransferases and demethylases fine-tune gene expression acting at hundreds or thousands of genes. Moreover, in mammals, H3K4 methyltransferases appear as pairs of paralogs that are believed to work redundantly (Glaser et al., 2009). For instance, whereas loss of Mll1 in fibroblasts had limited effects on H3K4me3 levels at Hox genes, loss of menin, which simultaneously affects MLL1- and MLL4-containing complexes, had a much broader impact (Wang et al., 2009).

Our data do not contradict these notions but imply that each H3K4 methyltransferase in a pair of paralogs also acquired specific and nonredundant functions. Data obtained with Wbp7 suggest at least two different scenarios related to specificity. First, a given H3K4 methyltransferase may exert a dominant role in controlling H3K4me3 in a specific cell type, as in the case of Wbp7 globally controlling H3K4me3 in oocytes (Andreu-Vieyra et al., 2010). Second, one individual methyltransferase, despite controlling H3K4 methylation at a large number of genomic locations, may impact crucial biological functions by selectively affecting the expression of one or a few genes essential for a specific pathway, as shown in this study. In this context, an intriguing observation is that the only gene strongly dependent on Wbp7 for expression in ES cells, *Magohb*, is

dependent on Wbp7 in macrophages as well. Therefore, Wbp7 is connected to the expression of this specific gene independently of the differentiation state of the cell, a result consistent with the idea of an extreme functional specialization of a subset of histone methyltransferases.

In conclusion, our mechanistic analysis of the transcriptional and epigenomic phenotype of Wbp7-deficient macrophages revealed that a housekeeping biosynthetic pathway essential for membrane localization of hundreds of molecules, including a coreceptor important for microbial recognition, is under tight and nonredundant control of a single H3K4 methyltransferase, which is otherwise dispensable for viability of adult mice.

EXPERIMENTAL PROCEDURES

Wbp7-Deficient Mice

Animal experiments were performed in accordance with the Italian Laws (D.L.vo 116/92 and following additions), which enforce EU 86/609 Directive. The Wbp7 floxed allele has been described (Glaser et al., 2006, 2009). The two loxP sites flank the 73 bp of *Wbp7* exon 2 and recombination leads to a frame shift and the generation of a premature stop codon. *Wbp7*$^{fl/fl}$ mice were crossed to Rosa26-CreERT2$^{+/-}$ mice and Cre was activated by gavage feeding of 5 mg tamoxifen (Sigma T5648) dissolved in peanut oil (Sigma P2144) for 5 consecutive days. Mice were sacrificed and bone marrow cells isolated 7–10 days after tamoxifen treatment. Efficiency of recombination was evaluated by Taqman assay (Figure S1A).

Cell Culture and Retroviral Infections

Macrophage cultures and retroviral infections were carried out as described (De Santa et al., 2007). LPS from *E. coli* serotype EH100 (Alexis) was used at 10 ng/ml unless otherwise indicated. The cDNA encoding Flag-tagged Pigp (NM_001159616) was obtained by standard cloning whereas the cDNA encoding CD14 fused to the transmembrane domain of mouse TLR4 was obtained by in vitro gene synthesis (MWG). Both cDNAs were subcloned into pMSCV-puro (Clontech).

Quantitative RT-PCR

RNA was extracted from macrophages with Trizol (Invitrogen) and reverse transcribed with random hexamers. Primers sequences are in Table S5.

FACS Analysis

Cells were stained with the following antibodies: F4/80 (Abcam ab6640; 1:50 dilution); biotin-labeled CD11b (BD #557395; 1:50 dilution) detected with streptavidin-PE-Cy5 (BD #554062); FITC-labeled CD14 (Abcam ab65087, 1:50 dilution); uPAR (a gift from N. Sidenius); and fluorescently labeled aerolysin (FLAER-Alexa488, Pinewood Scientific) at a concentration of 50 nM. The TLR4 antibody is a kind gift of J. Kagan (Harvard Medical School). The cells were analyzed by FACScalibur 4 or 10 channel flow cytometer (BD Biosciences).

Chromatin Immunoprecipitation and Sequencing

ChIP experiments were carried out as described starting from 2 × 10^7 cells (Ghisletti et al., 2010). Lysates were immunoprecipitated with 5 μg of H3K4me3 antibody (Active Motif #39159), 10 μg of H3K27me3 antibody (Active motif #39155), or menin antibody (Bethyl Labs., A300-105A). Antibodies were prebound to G protein-coupled paramagnetic beads (Dynabeads) in PBS/BSA 0.5% and incubated with lysates overnight. Beads were washed six times in a modified RIPA buffer (50 mM HEPES [pH 7.6], 500 mM LiCl, 1 mM EDTA, 1% NP-40, 0.7% Na-deoxycholate) and once in TE containing 50 mM NaCl. DNA was eluted in TE-2% SDS and crosslinks reversed by incubation overnight at 65°C. DNA was then purified by Qiaquick columns (QIAGEN) and quantified with PicoGreen (Invitrogen). Yield was ~10 ng/10^7 cells for H3K4me3. For validation by ChIP-QPCR, 0.4 μl of purified DNA was used for amplification on an ABI 7500 machine. Primers used for ChIP QPCR are in Table S5. ChIP DNA was prepared for Solexa 2G sequencing as described (Ghisletti et al., 2010). DNA quantified both with an Agilent Bioanalyzer and Picogreen was diluted to 10 nM. Cluster generation was performed and loaded into individual lanes of a flow cell (4 pmoles/sample).

A detailed description of the computational analyses is provided in the Supplemental Information. Statistics referring to the sequencing runs are in Table S6.

cDNA Microarrays

A biological triplicate was used for cDNA microarray analyses. RNA was purified with an RNeasy-QIAGEN kit. Quality analysis of total RNA, cRNA synthesis, hybridization, and data extraction were performed at the Cogentech Microarray Core Facility. The mouse gene ST1.0 Affymetrix array (Affymetrix) was used for gene expression screening. Data analysis is described in the Supplemental Information.

Immunoblot

The following antibodies were used: IκBα (Santa Cruz, sc-371), phospho-IKKa (S176, S180) (Upstate, #07-837), phospho-JNK (T183, Y185) (CST, #9251), JNK (CST, #9252), ERK1 (Santa Cruz, sc-94), phospho-ERK1/2 (E10) (CST, #9106), phospho-IRF3 (CST, #4947), IRF3 (CST #4302), and Tubulin (Sigma, T9026). For quantified images, secondary IRDye antibodies from Li-Cor were utilized (cat. no. 926-68021 and 926-32210).

ACCESSION NUMBERS

Raw data sets are available for download at the Gene Expression Omnibus (GEO) database (http://www.ncbi.nlm.nih.gov/gds/) under the accession number GSE30973, which comprises expression data (GSE30971) and ChIP-seq data (GSE30972).

SUPPLEMENTAL INFORMATION

Supplemental Information includes Supplemental Discussion, Supplemental Experimental Procedures, six figures, and six tables and can be found with this article online at doi:10.1016/j.immuni.2012.02.016.

ACKNOWLEDGMENTS

We thank B. Amati for critically reading this manuscript; N. Sidenius (IFOM, Milan) and J. Kagan (Harvard Medical School, Boston, MA) for antibodies; and G. Bucci (Cogentech, Milan) for initial microarray data analysis. This work was supported by the FP6 program of the European Community (Marie Curie Excellence Grant Trans-Tar to G.N.), the Italian Association for Research on Cancer, AIRC (G.N. and G.T.), the European Research Council (ERC, project *NORM*; G.N.), and the Italian Health Ministry (G.T.).

Received: October 19, 2011
Revised: January 20, 2012
Accepted: February 4, 2012
Published online: April 5, 2012

REFERENCES

Andreu-Vieyra, C.V., Chen, R., Agno, J.E., Glaser, S., Anastassiadis, K., Stewart, A.F., and Matzuk, M.M. (2010). MLL2 is required in oocytes for bulk histone 3 lysine 4 trimethylation and transcriptional silencing. PLoS Biol. *8*, 8.

Ayton, P., Sneddon, S.F., Palmer, D.B., Rosewell, I.R., Owen, M.J., Young, B., Presley, R., and Subramanian, V. (2001). Truncation of the Mll gene in exon 5 by gene targeting leads to early preimplantation lethality of homozygous embryos. Genesis *30*, 201–212.

Barski, A., Cuddapah, S., Cui, K., Roh, T.Y., Schones, D.E., Wang, Z., Wei, G., Chepelev, I., and Zhao, K. (2007). High-resolution profiling of histone methylations in the human genome. Cell *129*, 823–837.

Baumann, C.L., Aspalter, I.M., Sharif, O., Pichlmair, A., Blüml, S., Grebien, F., Bruckner, M., Pasierbek, P., Aumayr, K., Planyavsky, M., et al. (2010). CD14 is a coreceptor of Toll-like receptors 7 and 9. J. Exp. Med. *207*, 2689–2701.

Bernstein, B.E., Kamal, M., Lindblad-Toh, K., Bekiranov, S., Bailey, D.K., Huebert, D.J., McMahon, S., Karlsson, E.K., Kulbokas, E.J., 3rd, Gingeras, T.R., et al. (2005). Genomic maps and comparative analysis of histone modifications in human and mouse. Cell *120*, 169–181.

Blasi, F., and Sidenius, N. (2010). The urokinase receptor: focused cell surface proteolysis, cell adhesion and signaling. FEBS Lett. *584*, 1923–1930.

Boyer, L.A., Plath, K., Zeitlinger, J., Brambrink, T., Medeiros, L.A., Lee, T.I., Levine, S.S., Wernig, M., Tajonar, A., Ray, M.K., et al. (2006). Polycomb complexes repress developmental regulators in murine embryonic stem cells. Nature *441*, 349–353.

Bracken, A.P., Dietrich, N., Pasini, D., Hansen, K.H., and Helin, K. (2006). Genome-wide mapping of Polycomb target genes unravels their roles in cell fate transitions. Genes Dev. *20*, 1123–1136.

Brodsky, R.A., Mukhina, G.L., Li, S., Nelson, K.L., Chiurazzi, P.L., Buckley, J.T., and Borowitz, M.J. (2000). Improved detection and characterization of paroxysmal nocturnal hemoglobinuria using fluorescent aerolysin. Am. J. Clin. Pathol. *114*, 459–466.

Cho, Y.W., Hong, T., Hong, S., Guo, H., Yu, H., Kim, D., Guszczynski, T., Dressler, G.R., Copeland, T.D., Kalkum, M., and Ge, K. (2007). PTIP associates with MLL3- and MLL4-containing histone H3 lysine 4 methyltransferase complex. J. Biol. Chem. *282*, 20395–20406.

Cloos, P.A., Christensen, J., Agger, K., and Helin, K. (2008). Erasing the methyl mark: histone demethylases at the center of cellular differentiation and disease. Genes Dev. *22*, 1115–1140.

De Santa, F., Totaro, M.G., Prosperini, E., Notarbartolo, S., Testa, G., and Natoli, G. (2007). The histone H3 lysine-27 demethylase Jmjd3 links inflammation to inhibition of polycomb-mediated gene silencing. Cell *130*, 1083–1094.

De Santa, F., Narang, V., Yap, Z.H., Tusi, B.K., Burgold, T., Austenaa, L., Bucci, G., Caganova, M., Notarbartolo, S., Casola, S., et al. (2009). Jmjd3 contributes to the control of gene expression in LPS-activated macrophages. EMBO J. *28*, 3341–3352.

Diep, D.B., Nelson, K.L., Raja, S.M., Pleshak, E.N., and Buckley, J.T. (1998). Glycosylphosphatidylinositol anchors of membrane glycoproteins are binding determinants for the channel-forming toxin aerolysin. J. Biol. Chem. *273*, 2355–2360.

Ernst, P., Fisher, J.K., Avery, W., Wade, S., Foy, D., and Korsmeyer, S.J. (2004a). Definitive hematopoiesis requires the mixed-lineage leukemia gene. Dev. Cell *6*, 437–443.

Ernst, P., Mabon, M., Davidson, A.J., Zon, L.I., and Korsmeyer, S.J. (2004b). An Mll-dependent Hox program drives hematopoietic progenitor expansion. Curr. Biol. *14*, 2063–2069.

Foster, S.L., Hargreaves, D.C., and Medzhitov, R. (2007). Gene-specific control of inflammation by TLR-induced chromatin modifications. Nature *447*, 972–978.

Frontini, M., Soutoglou, E., Argentini, M., Bole-Feysot, C., Jost, B., Scheer, E., and Tora, L. (2005). TAF9b (formerly TAF9L) is a bona fide TAF that has unique and overlapping roles with TAF9. Mol. Cell. Biol. *25*, 4638–4649.

Ghisletti, S., Barozzi, I., Mietton, F., Polletti, S., De Santa, F., Venturini, E., Gregory, L., Lonie, L., Chew, A., Wei, C.L., et al. (2010). Identification and characterization of enhancers controlling the inflammatory gene expression program in macrophages. Immunity *32*, 317–328.

Giorgetti, L., Siggers, T., Tiana, G., Caprara, G., Notarbartolo, S., Corona, T., Pasparakis, M., Milani, P., Bulyk, M.L., and Natoli, G. (2010). Noncooperative interactions between transcription factors and clustered DNA binding sites enable graded transcriptional responses to environmental inputs. Mol. Cell *37*, 418–428.

Glaser, S., Schaft, J., Lubitz, S., Vintersten, K., van der Hoeven, F., Tufteland, K.R., Aasland, R., Anastassiadis, K., Ang, S.L., and Stewart, A.F. (2006). Multiple epigenetic maintenance factors implicated by the loss of Mll2 in mouse development. Development *133*, 1423–1432.

Glaser, S., Lubitz, S., Loveland, K.L., Ohbo, K., Robb, L., Schwenk, F., Seibler, J., Roellig, D., Kranz, A., Anastassiadis, K., and Stewart, A.F. (2009). The histone 3 lysine 4 methyltransferase, Mll2, is only required briefly in development and spermatogenesis. Epigenetics Chromatin *2*, 5.

Guenther, M.G., Levine, S.S., Boyer, L.A., Jaenisch, R., and Young, R.A. (2007). A chromatin landmark and transcription initiation at most promoters in human cells. Cell *130*, 77–88.

Haziot, A., Ferrero, E., Köntgen, F., Hijiya, N., Yamamoto, S., Silver, J., Stewart, C.L., and Goyert, S.M. (1996). Resistance to endotoxin shock and reduced dissemination of gram-negative bacteria in CD14-deficient mice. Immunity *4*, 407–414.

Huang, Y., Fang, J., Bedford, M.T., Zhang, Y., and Xu, R.M. (2006). Recognition of histone H3 lysine-4 methylation by the double tudor domain of JMJD2A. Science *312*, 748–751.

Hughes, C.M., Rozenblatt-Rosen, O., Milne, T.A., Copeland, T.D., Levine, S.S., Lee, J.C., Hayes, D.N., Shanmugam, K.S., Bhattacharjee, A., Biondi, C.A., et al. (2004). Menin associates with a trithorax family histone methyltransferase complex and with the hoxc8 locus. Mol. Cell *13*, 587–597.

Jenuwein, T., and Allis, C.D. (2001). Translating the histone code. Science *293*, 1074–1080.

Kim, J., Daniel, J., Espejo, A., Lake, A., Krishna, M., Xia, L., Zhang, Y., and Bedford, M.T. (2006). Tudor, MBT and chromo domains gauge the degree of lysine methylation. EMBO Rep. *7*, 397–403.

Kim, J., Guermah, M., McGinty, R.K., Lee, J.S., Tang, Z., Milne, T.A., Shilatifard, A., Muir, T.W., and Roeder, R.G. (2009). RAD6-mediated transcription-coupled H2B ubiquitylation directly stimulates H3K4 methylation in human cells. Cell *137*, 459–471.

Kinoshita, T., Fujita, M., and Maeda, Y. (2008). Biosynthesis, remodelling and functions of mammalian GPI-anchored proteins: recent progress. J. Biochem. *144*, 287–294.

Klose, R.J., and Zhang, Y. (2007). Regulation of histone methylation by demethylimination and demethylation. Nat. Rev. Mol. Cell Biol. *8*, 307–318.

Klymenko, T., and Müller, J. (2004). The histone methyltransferases Trithorax and Ash1 prevent transcriptional silencing by Polycomb group proteins. EMBO Rep. *5*, 373–377.

Kornberg, R.D., and Lorch, Y. (1999). Twenty-five years of the nucleosome, fundamental particle of the eukaryote chromosome. Cell *98*, 285–294.

Kouzarides, T. (2007). Chromatin modifications and their function. Cell *128*, 693–705.

Lachner, M., O'Carroll, D., Rea, S., Mechtler, K., and Jenuwein, T. (2001). Methylation of histone H3 lysine 9 creates a binding site for HP1 proteins. Nature *410*, 116–120.

Lee, M.S., and Kim, Y.J. (2007). Signaling pathways downstream of pattern-recognition receptors and their cross talk. Annu. Rev. Biochem. *76*, 447–480.

Lee, J.H., and Skalnik, D.G. (2008). Wdr82 is a C-terminal domain-binding protein that recruits the Setd1A Histone H3-Lys4 methyltransferase complex to transcription start sites of transcribed human genes. Mol. Cell. Biol. *28*, 609–618.

Lee, J.D., Kato, K., Tobias, P.S., Kirkland, T.N., and Ulevitch, R.J. (1992). Transfection of CD14 into 70Z/3 cells dramatically enhances the sensitivity to complexes of lipopolysaccharide (LPS) and LPS binding protein. J. Exp. Med. *175*, 1697–1705.

Lee, H.K., Dunzendorfer, S., Soldau, K., and Tobias, P.S. (2006a). Double-stranded RNA-mediated TLR3 activation is enhanced by CD14. Immunity *24*, 153–163.

Lee, T.I., Jenner, R.G., Boyer, L.A., Guenther, M.G., Levine, S.S., Kumar, R.M., Chevalier, B., Johnstone, S.E., Cole, M.F., Isono, K., et al. (2006b). Control of developmental regulators by Polycomb in human embryonic stem cells. Cell *125*, 301–313.

Mikkelsen, T.S., Ku, M., Jaffe, D.B., Issac, B., Lieberman, E., Giannoukos, G., Alvarez, P., Brockman, W., Kim, T.K., Koche, R.P., et al. (2007). Genome-wide maps of chromatin state in pluripotent and lineage-committed cells. Nature *448*, 553–560.

Miller, T., Krogan, N.J., Dover, J., Erdjument-Bromage, H., Tempst, P., Johnston, M., Greenblatt, J.F., and Shilatifard, A. (2001). COMPASS: a complex of proteins associated with a trithorax-related SET domain protein. Proc. Natl. Acad. Sci. USA *98*, 12902–12907.

Pavri, R., Zhu, B., Li, G., Trojer, P., Mandal, S., Shilatifard, A., and Reinberg, D. (2006). Histone H2B monoubiquitination functions cooperatively with FACT to regulate elongation by RNA polymerase II. Cell *125*, 703–717.

Peña, P.V., Davrazou, F., Shi, X., Walter, K.L., Verkhusha, V.V., Gozani, O., Zhao, R., and Kutateladze, T.G. (2006). Molecular mechanism of histone H3K4me3 recognition by plant homeodomain of ING2. Nature *442*, 100–103.

Peters, A.H., O'Carroll, D., Scherthan, H., Mechtler, K., Sauer, S., Schöfer, C., Weipoltshammer, K., Pagani, M., Lachner, M., Kohlmaier, A., et al. (2001). Loss of the Suv39h histone methyltransferases impairs mammalian heterochromatin and genome stability. Cell *107*, 323–337.

Peters, A.H., Kubicek, S., Mechtler, K., O'Sullivan, R.J., Derijck, A.A., Perez-Burgos, L., Kohlmaier, A., Opravil, S., Tachibana, M., Shinkai, Y., et al. (2003). Partitioning and plasticity of repressive histone methylation states in mammalian chromatin. Mol. Cell *12*, 1577–1589.

Ruthenburg, A.J., Allis, C.D., and Wysocka, J. (2007). Methylation of lysine 4 on histone H3: intricacy of writing and reading a single epigenetic mark. Mol. Cell *25*, 15–30.

Santos-Rosa, H., Schneider, R., Bannister, A.J., Sherriff, J., Bernstein, B.E., Emre, N.C., Schreiber, S.L., Mellor, J., and Kouzarides, T. (2002). Active genes are tri-methylated at K4 of histone H3. Nature *419*, 407–411.

Sims, R.J., 3rd, Millhouse, S., Chen, C.F., Lewis, B.A., Erdjument-Bromage, H., Tempst, P., Manley, J.L., and Reinberg, D. (2007). Recognition of trimethylated histone H3 lysine 4 facilitates the recruitment of transcription postinitiation factors and pre-mRNA splicing. Mol. Cell *28*, 665–676.

Smith, E., Lin, C., and Shilatifard, A. (2011). The super elongation complex (SEC) and MLL in development and disease. Genes Dev. *25*, 661–672.

Subramanian, A., Tamayo, P., Mootha, V.K., Mukherjee, S., Ebert, B.L., Gillette, M.A., Paulovich, A., Pomeroy, S.L., Golub, T.R., Lander, E.S., and Mesirov, J.P. (2005). Gene set enrichment analysis: a knowledge-based approach for interpreting genome-wide expression profiles. Proc. Natl. Acad. Sci. USA *102*, 15545–15550.

Tachibana, M., Sugimoto, K., Nozaki, M., Ueda, J., Ohta, T., Ohki, M., Fukuda, M., Takeda, N., Niida, H., Kato, H., and Shinkai, Y. (2002). G9a histone methyltransferase plays a dominant role in euchromatic histone H3 lysine 9 methylation and is essential for early embryogenesis. Genes Dev. *16*, 1779–1791.

Tachibana, M., Ueda, J., Fukuda, M., Takeda, N., Ohta, T., Iwanari, H., Sakihama, T., Kodama, T., Hamakubo, T., and Shinkai, Y. (2005). Histone methyltransferases G9a and GLP form heteromeric complexes and are both crucial for methylation of euchromatin at H3-K9. Genes Dev. *19*, 815–826.

Testa, G., Schaft, J., van der Hoeven, F., Glaser, S., Anastassiadis, K., Zhang, Y., Hermann, T., Stremmel, W., and Stewart, A.F. (2004). A reliable lacZ expression reporter cassette for multipurpose, knockout-first alleles. Genesis *38*, 151–158.

Thomson, J.P., Skene, P.J., Selfridge, J., Clouaire, T., Guy, J., Webb, S., Kerr, A.R., Deaton, A., Andrews, R., James, K.D., et al. (2010). CpG islands influence chromatin structure via the CpG-binding protein Cfp1. Nature *464*, 1082–1086.

Wang, P., Lin, C., Smith, E.R., Guo, H., Sanderson, B.W., Wu, M., Gogol, M., Alexander, T., Seidel, C., Wiedemann, L.M., et al. (2009). Global analysis of H3K4 methylation defines MLL family member targets and points to a role for MLL1-mediated H3K4 methylation in the regulation of transcriptional initiation by RNA polymerase II. Mol. Cell. Biol. *29*, 6074–6085.

Watanabe, R., Murakami, Y., Marmor, M.D., Inoue, N., Maeda, Y., Hino, J., Kangawa, K., Julius, M., and Kinoshita, T. (2000). Initial enzyme for glycosylphosphatidylinositol biosynthesis requires PIG-P and is regulated by DPM2. EMBO J. *19*, 4402–4411.

Wright, S.D., Ramos, R.A., Tobias, P.S., Ulevitch, R.J., and Mathison, J.C. (1990). CD14, a receptor for complexes of lipopolysaccharide (LPS) and LPS binding protein. Science *249*, 1431–1433.

Wu, M., Wang, P.F., Lee, J.S., Martin-Brown, S., Florens, L., Washburn, M., and Shilatifard, A. (2008). Molecular regulation of H3K4 trimethylation by Wdr82, a component of human Set1/COMPASS. Mol. Cell. Biol. *28*, 7337–7344.

Yagi, H., Deguchi, K., Aono, A., Tani, Y., Kishimoto, T., and Komori, T. (1998). Growth disturbance in fetal liver hematopoiesis of Mll-mutant mice. Blood *92*, 108–117.

Yu, B.D., Hess, J.L., Horning, S.E., Brown, G.A., and Korsmeyer, S.J. (1995). Altered Hox expression and segmental identity in Mll-mutant mice. Nature *378*, 505–508.

Zanoni, I., Ostuni, R., Capuano, G., Collini, M., Caccia, M., Ronchi, A.E., Rocchetti, M., Mingozzi, F., Foti, M., Chirico, G., et al. (2009). CD14 regulates the dendritic cell life cycle after LPS exposure through NFAT activation. Nature *460*, 264–268.

Zanoni, I., Ostuni, R., Marek, L.R., Barresi, S., Barbalat, R., Barton, G.M., Granucci, F., and Kagan, J.C. (2011). CD14 controls the LPS-induced endocytosis of Toll-like receptor 4. Cell *147*, 868–880.